Preprints (www.preprints.org) | NOT PEER-REVIEWED | Posted: 10 December 2021 doi:10.20944/preprints202112.0182.v1

Article

Superionic solid electrolyte $Li_7La_3Zr_2O_{12}$ synthesis and thermodynamics for application in all-solid-state lithium-ion batteries

Anatoliy Popovich [1], Pavel Novikov [1], Qingsheng Wang [2] and Daniil Aleksandrov [1,*]

[1] Peter the Great St. Petersburg Polytechnic university, Saint Petersburg, Russia; director@immet.spbstu.ru;
[2] CHN/RUS New Energy and Material Technology Research Institute, Changxing, China; envbattery@yandex.ru;
* Correspondence: aleksandrov_ds@spbstu.ru

Abstract: Solid-state reaction was used for $Li_7La_3Zr_2O_{12}$ material synthesis from Li_2CO_3, La_2O_3 and ZrO_2 powders. Phase investigation by XRD, SEM and EDS methods of $Li_7La_3Zr_2O_{12}$ were carried out. The molar heat capacity of $Li_7La_3Zr_2O_{12}$ at constant pressure in the temperature range 298-800 K should be calculated as $C_{p,m} = 518.135+0.599 \times T - 8.339 \times T^{-2}$, where T is absolute temperature, . Thermodynamic characteristics of $Li_7La_3Zr_2O_{12}$ were determined as next: entropy $S^0_{298} = 362.3$ J mol^{-1} K^{-1}, molar enthalpy of dissolution $\Delta_d H_{LLZO} = -1471.73 \pm 29.39$ kJ mol^{-1}, the standard enthalpy of formation from elements $\Delta_f H^0 = -9327.65 \pm 7.9$ kJ mol^{-1}, the standard Gibbs free energy of formation $\Delta_f G^0_{298} = -9435.6$ kJ mol^{-1}.

Keywords: lithium-ion battery; solid-state electrolyte; lithium-ion thermodynamics; solid-state synthesis

1. Introduction

The commercial history of lithium-ion battery has started at 1991 by Sony [1]. Since, a lot of efforts were directed to improve electrochemical performance of lithium-ion batteries [2]. One of the perspective decisions to stabilize lithium-ion battery electrochemical characteristics and safety is apply solid-state inorganic electrolyte instead of liquid organic electrolyte as traditional electrolyte for commercial lithium-ion batteries [3]-[7]. Some solid-state electrolytes have high ionic conductivity in an order of magnitude of ~10^{-3} S cm^{-1} [8] in comparison to liquid electrolyte [9].

Between all types of the solid-state electrolytes (perovskite, NASICON- and LISICON-type, LATP- and LAGP-type, garnet, sulfide and halide electrolytes, etc. [8]) garnet-type electrolytes have the most attractive electrochemical performance in combination with manufacture costs and simplicity in commercial application. Garnet-type $Li_7La_3Zr_2O_{12}$ (LLZO) solid-state electrolyte has two modifications: cubic and tetragonal. The ionic conductivity is ~10^{-4} – 10^{-3} S cm^{-1} and ~ 10^{-7} – 10^{-6} S cm^{-1}, respectively [10].

LLZO solid-state electrolyte attracts high attention due to its' relatively high electrochemical properties. Though, LLZO has lower ionic conductivity in comparison with organic liquid electrolyte (~10^{-4} versus ~10^{-2} S cm^{-1}, respectively [9]), it provides high safety performance, high chemical stability against metallic lithium, a wide electrochemical potential window, low electronic conductivity, high stability with moisture in air; LLZO prevents lithium dendrites growth due to high mechanical strength [11]-[15].

Since as LLZO has been first synthesized by *Murugan* et al. [16], it was investigated to improve its' chemical and structure stability, long cycle life, electrode/solid electrolyte interface interactions, high energy density at room temperature. Thus, heterovalent substitution/doping with Al^{3+} from alumina crucible (or intentional incorporation) during synthesis process allow enhance the ionic conductivity up to ~10^{-3} S cm^{-1}, but it cause in higher activation energy of lithium ion conduction, which limits Li^+ mobility [17]-[24]. Doped with Ga^{3+} also as Al^{3+} stabilize structure of LLZO [25]-[32]. The substitution of Zr^{4+} with Ta^{5+} ions allow increase of the ionic conductivity, stabilize the cubic structure,

© 2021 by the author(s). Distributed under a Creative Commons CC BY license.

Preprints (www.preprints.org) | NOT PEER-REVIEWED | Posted: 10 December 2021 doi:10.20944/preprints202112.0182.v1

improve lithium-ion transport, lithium dendrite growth prevention and current density [33]-[38]. Totally, mentioned above elements improves electrochemical and structure stability, increase the ionic conductivity, prevent lithium dendrite growth and penetration at the solid electrolyte structure.

In this work, synthesis, structure studies and thermodynamics calculations of tetragonal $Li_7La_3Zr_2O_{12}$ were performed.

2. Materials and Methods

Tetragonal LLZO electrolyte was produced by solid-state synthesis as the one of the commonly used synthesis methods for investigation and mass manufacture [39]-[47]. Initial materials Li_2CO_3 (Xilong Sci., 99%), La_2O_3 (ReLAB, 99.99%) and ZrO_2 (Sinopharm, 99.9%) in stoichiometric ratio were used as source for Li, La and Zr, respectively. Excess 10 wt. % of lithium was initially added to precursor to avoid lithium loss during synthesis process at high temperature. Lanthanum oxide was preliminarily dried at 900°C for 24 h. Mentioned materials mechanically milled at agate mortar and then dissolved at acetic acid with following magnetic stirring at 90°C for 12 h to provide homogeneous solution. Excess acetic acid was evaporated at 110°C to get dry precursor powder. Dried precursor has been mechanically milled at agate mortar and put into alumina crucible for heat treatment. Muffle furnace Nabertherm™ was used for solid-state reaction at air atmosphere. Firstly, precursor was slowly heated (heat rate was 0.5°C/min) to 130°C for 3 h to evaporate remaining acetic acid. Then, precursor was heated (heat rate was 2°C/min) to 900°C for 8 h to provide solid-state reaction.

Solid-state reaction proceeds according to next formula:

$$4ZrO_2 + 3La_2O_3 + 7Li_2CO_3 = 2Li_7La_3Zr_2O_{12} + 7CO_2 \quad (1)$$

X-ray diffraction structural analysis (XRD) was performed by Bruker D8 Advance equipment (diffraction angle step was 0.02°, Cu K_α-radiation). Rietveld method was used for structure refinement. Diffraction angles for synthesized LLZO powder were set from 15° to 60° (2Θ).

Images of microstructure performance of LLZO powder were performed with scanning electron microscope (SEM) Tescan MAIA3 with secondary electron detection. Bruker XFlash 6-10 was used for energy-dispersive X-ray spectroscopy (EDS).

TAM IV Microcalorimeter was used for calorimetric investigation. Measurement parameters were next: temperature is 298 K, volume of cell is 20 ml. Aqueous solution of 1 mol dm^{-3} HCl was filled in the ampoule at calorimetric cell. Dissolution process of LLZO powder has been started after thermal equilibrium was established. Dissolution enthalpy value was obtained from thermoelectromotive force data during the dissolution process, providing the heat dissolution curve.

3. Results

XRD pattern of synthesized LLZO is shown at Figure 1. According to diffraction data, LLZO has $I4_1/acd$ space group. Vertical lines at the bottom are related to PDF #00-064-0140. The peaks indexes and interplanar distances are shown at Supplementary. Synthesized material contains 4 wt. % of La_2O_3 impurity after solid-state reaction.

Preprints (www.preprints.org) | NOT PEER-REVIEWED | Posted: 10 December 2021 doi:10.20944/preprints202112.0182.v1

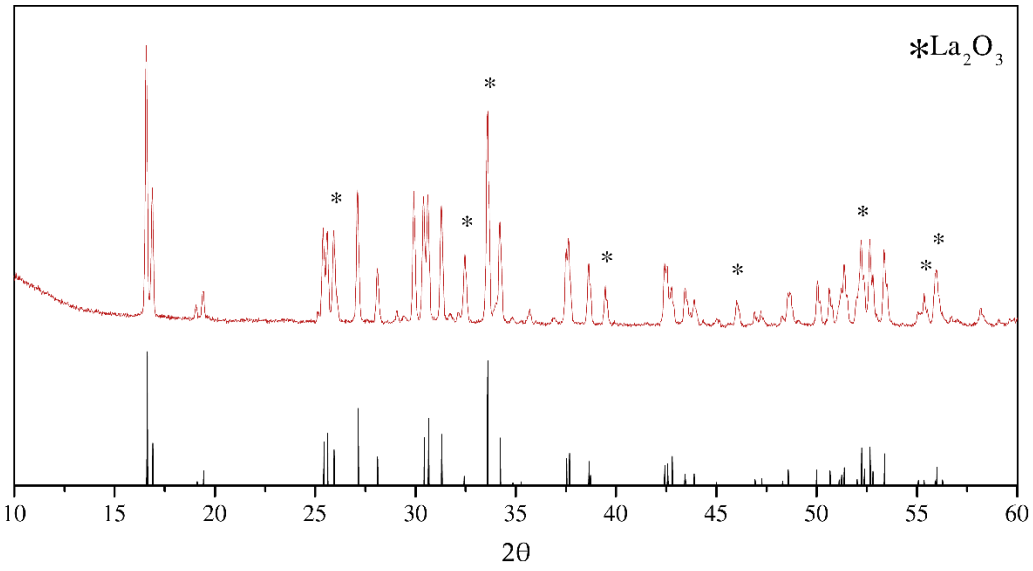

Figure 1. X-ray diffraction pattern of synthesized tetragonal $Li_7La_3Zr_2O_{12}$ by solid-state reaction. Bottom vertical lines belong to PDF #00-064-0140.

SEM images of LLZO powder are shown at Figure 2, made at 2x, 3.5x, 10x and 11.5x magnification, respectively. All images were performed at 10 keV landing energy.

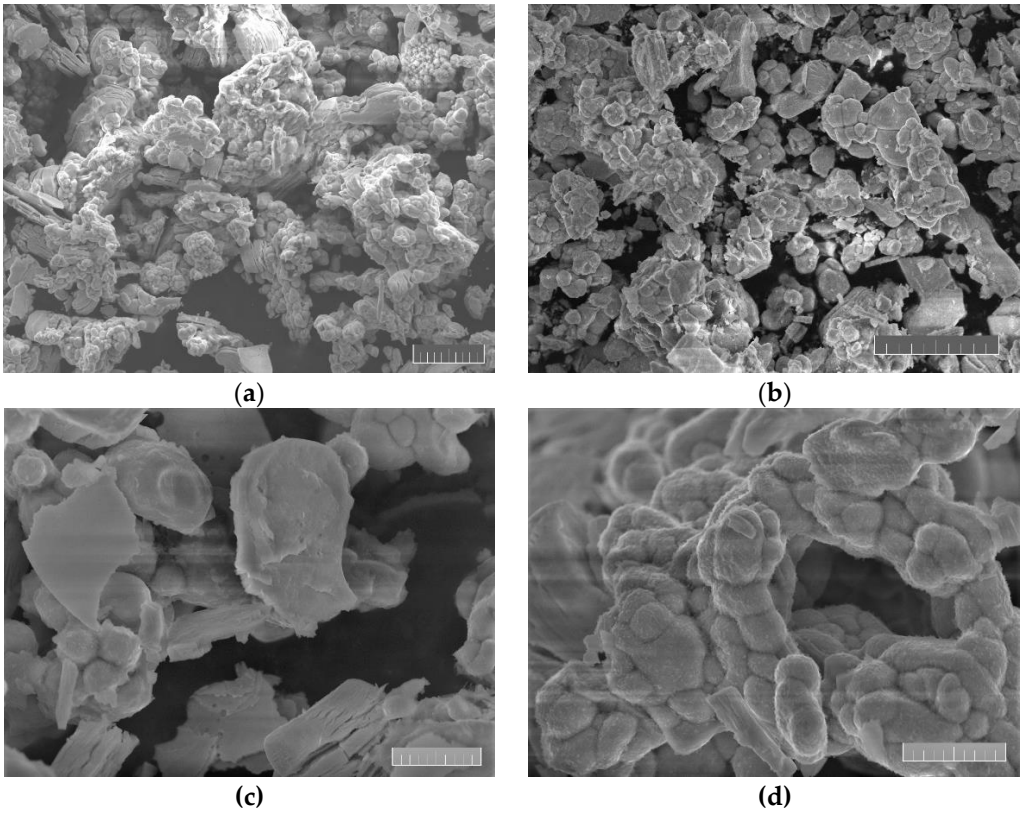

Figure 2. SEM images of synthesized LLZO powder at different magnification. The scale bar is (a), (b) 20 μm and (c), (d) 5 μm long.

EDS spectra images are shown at Figure 3. The scale bar is 80 μm long for all images (a)-(d). Green frame at Figure 3, (a) shows EDS analyzing field. Figures 3,(b)-(d) shows elements distribution for La, Zr, O and C (b), La (c) and Zr (d) elements, respectively. The elements at Figure 3 are evenly distributed. Carbon at Figure 3, (b) is electrically conductive carbon tape for sample holder. Elemental analysis of EDS spectra is shown at Table 1.

Preprints (www.preprints.org) | NOT PEER-REVIEWED | Posted: 10 December 2021 doi:10.20944/preprints202112.0182.v1

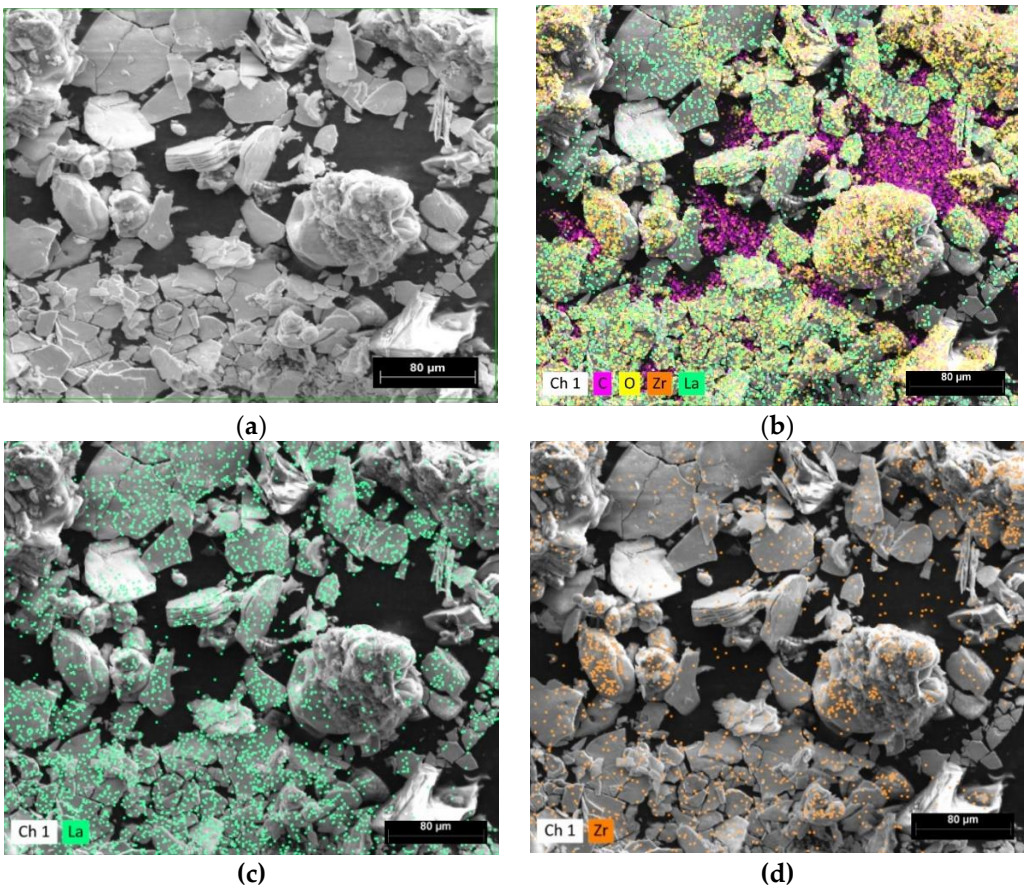

Figure 3. SEM images of synthesized LLZO powder at different magnification. The scale bar is (a), (b) 20 µm and (c), (d) 5 µm long.

EDS elemental analysis of LLZO powder shows lanthanum excess of solid electrolyte powder, expressed in terms of $Li_7La_3Zr_2O_{12}$ and La_2O_3 compounds. Elemental analysis based on Table 2 shows excess of 3.1 wt.% of lanthanum oxide (III).

Table 2. Elemental EDS analysis of $Li_7La_3Zr_2O_{12}$ powder.

Element	Mass, wt. %
Lanthanum	53.19
Oxygen	22.59
Zirconium	24.22

4. Discussion

4.1. The standard enthalpy of formation

The enthalpy of $Li_7La_3Zr_2O_{12}$ formation ($\Delta_{ox}H_{LLZO}$) from Li_2CO_3, La_2O_3 and ZrO_2 is calculated according to the equation (1) from Experimental section. The subscript *ox* means "oxides", that related to initial compounds of equation (1).

The following thermodynamic cycle was used for enthalpy calculation, Figure 4:

$$Li_7La_3Zr_2O_{12} + 24HCl_{(aq)} \rightarrow 7LiCl_{(aq)} + 3LaCl_{3(aq)} + 2ZrCl_{4(aq)} + 12H_2\uparrow + 6O_2\uparrow, \quad (2)$$

$$Li_2CO_3 + 2HCl_{(aq)} \rightarrow 2LiCl + CO_2 + H_2O, \quad (3)$$

$$La_2O_3 + 6HCl_{(aq)} \rightarrow 2LaCl_3 + 3H_2O, \quad (4)$$

$$ZrO_2 + 4HCl_{(aq)} \rightarrow ZrCl_4 + 2H_2O, \quad (5)$$

Preprints (www.preprints.org) | NOT PEER-REVIEWED | Posted: 10 December 2021 doi:10.20944/preprints202112.0182.v1

the subscript *(aq)* indicates "aqueous". The calorimeter was used for the standard enthalpy ($\Delta_d H_{LLZO}$) measurement. The received value after calorimetry measurement was equal to −1911 ± 37 J g^{-1}, Table 3.

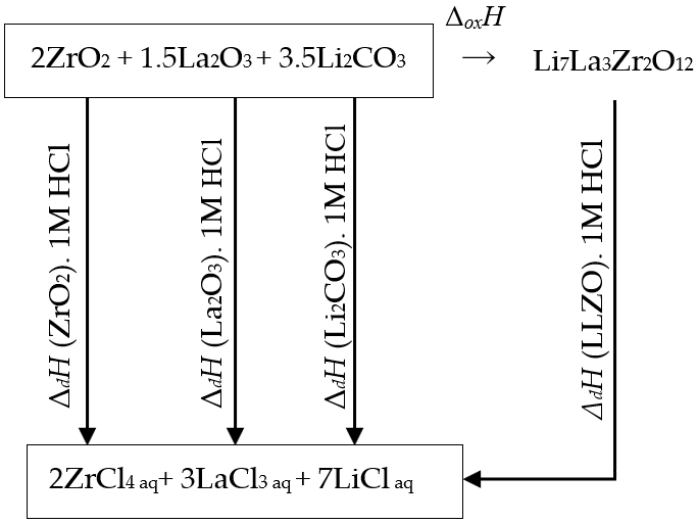

Figure 4. Thermochemical cycle scheme of LLZO dissolution in HCl.

It was shown in Experimental section, that LLZO has 3.1 wt. % of unreacted La_2O_3 impurity. Thereby, measured $\Delta_d H_{LLZO}$ should be recalculated considering the amount of La_2O_3:

$$\Delta_d H_{LLZO} = \frac{\Delta_d H_{LLZO+La2O3} - \omega \Delta_d H_{La2O3}}{1-\omega}, \quad (6)$$

ω – mass fraction of La_2O_3. It should be noted that enthalpies, mentioned at equation (6) are supposed to be specific, not molar. The recalculated value of the dissolution enthalpy of LLZO (with 3.1 wt.% of La_2O_3) is equal to -1 917.7 J g^{-1} or -1 607.75 kJ mol^{-1}, Table 3.

Table 3. Specific and molar enthalpies of dissolution values (1 mol dm^{-3} $HCl_{(aq)}$, T=298 K, p=101 kPa).

Compound	Specific enthalpy, J g^{-1}	Molar mass, g mol^{-1}	Molar enthalpy of dissolution, kJ mol^{-1}	Ref.
ZrO_2	- 2186 ± 19	123.222	-269.4 ± 2.34	this work
La_2O_3	- 1927 ± 13	325.837	-627.9 ± 4.23	this work
Li_2CO_3	- 683 ± 9	73.89	-50.5 ± 0.67	this work
$Li_7La_3Zr_2O_{12}$ (with La_2O_3 impurity)	- 1758 ± 34	-	-	this work
$Li_7La_3Zr_2O_{12}$	- 1752.6 ± 35	839.741	-1471.73 ± 29.39	this work (recalculated)

The resulting value of $\Delta_{ox} H_{LLZO}$ is obtained by next equation:

$$\Delta_{ox} H_{LLZO} = 2\Delta_d H_{ZrO2} + 1.5\Delta_d H_{La2O3} + 3.5\Delta_d H_{Li2CO3} - \Delta_d H_{LLZO} \quad (7)$$

The values of $\Delta_d H_{ZrO2}$, $\Delta_d H_{La2O3}$ and $\Delta_d H_{Li2CO3}$, measured by calorimetry method are shown at Table 3. The recalculated value of the enthalpy of dissolution of $Li_7La_3Zr_2O_{12}$ was used for $\Delta_{ox} H_{LLZO}$ evaluation. The value of $\Delta_{ox} H_{LLZO}$ by equation (7) is equal to -186.4 kJ mol^{-1}. Negative value of the enthalpy of $Li_7La_3Zr_2O_{12}$ formation indicate that $Li_7La_3Zr_2O_{12}$ is a stable phase and there is an energy benefit in the formation of $Li_7La_3Zr_2O_{12}$ from Li_2CO_3, La_2O_3 and ZrO_2. The values for various lithium zirconates were added to Table 3 to compare with measured and calculated values at this work. The value of the enthalpy

Preprints (www.preprints.org) | NOT PEER-REVIEWED | Posted: 10 December 2021 doi:10.20944/preprints202112.0182.v1

of formation from binary oxides $\Delta_{ox}H_{LLZO}$ has the same order as corresponding values for lithium zirconate compounds and complex oxides (Table 4), thus it can be concluded that measurements are correct.

Table 4. Standard enthalpies of formation of complex oxides from binary oxides ($\Delta_{ox}H^0$)

Compound	$\Delta_{ox}H^\circ_{298.15}$, kJ mol^{-1}	Reference
$Li_7La_3Zr_2O_{12}$ (s)	−186.4 ± 7.3	this work
Li_2ZrO_3 (s)	−304.1 ± 1.4	[48]
$Li_6Zr_2O_7$ (s)	−112.86	[49]
$La_2Zr_2O_7$ (s)	−135.6	[50]
Li_2TiO_3 (s)	−238.5 ± 1.5	[48]
$LiAlO_2$ (s)	−209.0 ± 3.2	[48]
$LiCoO_2$ (s)	−143.99 ± 1.38	[51]
$BaZrO_3$ (s)	−114.6	[52]

The subscripts (s) mean "solid".

Finally, the enthalpy of $Li_7La_3Zr_2O_{12}$ formation from elements can be calculated by formula:

$$\Delta_f H_{LLZO} = 3.5\Delta_f H_{Li2CO3} + 1.5\Delta_f H_{La2O3} + 2\Delta_f H_{ZrO2} + \Delta_{ox}H_{LLZO}. \quad (8)$$

Standard enthalpies for the calculation were taken from the handbook [53], Table 5.

Table 5. Standard enthalpies of formation from elements ($\Delta_f H^0$).

Compound	$\Delta_f H^\circ_{298.15}$, kJ mol^{-1}	Reference
Li_2CO_3 (s)	−1214.1 ± 1.0	[53]
La_2O_3 (s)	−1794.2 ± 2.0	[53]
ZrO_2 (s)	−1100.3 ± 0.7	[53]
$Li_7La_3Zr_2O_{12}$ (s)	−9327.65 ± 7.9	this work

The subscripts (s) mean "solid".

The calculated value of the formation enthalpy of $Li_7La_3Zr_2O_{12}$ by formula (8) is −9327.65 ± 7.9 kJ mol^{-1}, Table 5. The enthalpy of formation value, rated by Equation (8), can be recommended to use in further thermodynamic calculations of $Li_7La_3Zr_2O_{12}$ reactivity.

4.2. The isobaric heat capacity

The temperature dependence of the isobaric heat capacity of the $Li_7La_3Zr_2O_{12}$ is shown on Figure 5. According to XRD and EDS data (Figure 1 and Table 2, respectively), obtained powder material contains a certain amount of lanthanum oxide La_2O_3. This amount must be considered for calculating the heat capacity of the $Li_7La_3Zr_2O_{12}$. The impurity could appear after synthesis process as unreacted compound. The heat capacity of a two-phase system must be recalculated by additive consideration:

$$mC_p = m(LLZO)C_p(LLZO) + m(La_2O_3)C_p(La_2O_3), \quad (9)$$

C_p – a specific heat capacity (p=const), m is a mass. The sample mass consists of synthesized compound (LLZO) and impurity (La_2O_3). Thus, the heat capacity of $Li_7La_3Zr_2O_{12}$ is expressed from eq. (9) as:

$$C_p(LLZO) = \frac{mC_p - m(La_2O_3)C_p(La_2O_3)}{m(LLZO)} \quad (10)$$

The impurity compound weight can be recalculated from the sample total mass, with the known mass fraction of lanthanum oxide, $\omega(La_2O_3)$:

Preprints (www.preprints.org) | NOT PEER-REVIEWED | Posted: 10 December 2021 doi:10.20944/preprints202112.0182.v1

$$m(La_2O_3) = m\omega(La_2O_3) \quad (11)$$

and

$$m(LLZO) = m[1-\omega(La_2O_3)] \quad (12)$$

According to eq. (11) and (12), eq. (13) can be written as follows:

$$C_p(LLZO) = \frac{C_p - C_p(La_2O_3)\omega(La_2O_3)}{1-\omega(La_2O_3)} \quad (13)$$

Thereby, the heat capacity of LLZO can be calculated from the experimental data and heat capacity of La_2O_3 impurity. Dependence of La_2O_3 specific heat capacity from temperature is required for Equation (13) calculation. For this, tabular data required to define temperature dependence for the lanthanum oxide heat capacity [53]. The commonly used polynomial for the heat capacity (for 300-800 K in our case):

$$C_p = a + bT - cT^{-2} \quad (14)$$

where a, b, and c are empirical coefficients; T is the absolute temperature. The received coefficients for lanthanum oxide are: a = 119.604 J mol^{-1} K^{-1}, b = 14.514·10^{-3} J mol^{-1} K^{-2}, c = 13.452·10^{5} J mol^{-1} K. The heat capacity of LLZO for 300-800 K temperature range was recalculated using eq. (14) and (13) considering La_2O_3 impurity presence. According to XRD and EDS data (Figure 1 and Table 2, respectively) LLZO contains about 3.1±0.12 wt. % La_2O_3. Experimental and recalculated LLZO heat capacity is shown on Figure 5 and Table 6. Empirical values for heat capacity were calculated by Neumann-Kopp (N-K) rule. This rule prescribes to calculate the molar heat capacity of complex compound from the heat capacities of constituent elements by adding them in with compound stoichiometry. But this calculation method gives good results for room temperatures and rough results for high temperatures. For more accurate results binary compounds were used instead to single elements (accurate results are usually obtained for the same aggregate state of materials):

$$C_p(CO) = \sum n(BO)C_p(BO) \quad (15)$$

C_p is molar heat capacity (p=const), n is a stoichiometric coefficient, CO and BO are complex and binary oxide, respectively. For LLZO, eq. (15) can be written as (according to eq. (1)):

$$C_p\,(LLZO) = 3.5C_p\,(Li_2CO_3) + 1.5C_p\,(La_2O_3) + 2C_p\,(ZrO_2) \quad (16)$$

The temperature dependence of the heat capacity calculated from eq. (16) using tabular data [53] is also shown on Figure 5 and Table 6.

Table 6. The temperature dependence of experimental (exp.), recalculated by eq. (15) (rec.) and calculated by Neumann-Kopp (N-K) rule (eq. 16) heat capacities (Cp) of $Li_7La_3Zr_2O_{12}$ (s).

T, K	C_p(exp.), J K^{-1} mol^{-1}	C_p(rec.), J K^{-1} mol^{-1}	C_p(N-K), J K^{-1} mol^{-1}
300	126.9	124.1	621.1
400	134.1	132.6	708.1
500	146.3	144.3	778.8
600	160.5	158.3	843.1
700	173.8	171.9	904.3
800	183.3	180.7	964.0

Preprints (www.preprints.org) | NOT PEER-REVIEWED | Posted: 10 December 2021 doi:10.20944/preprints202112.0182.v1

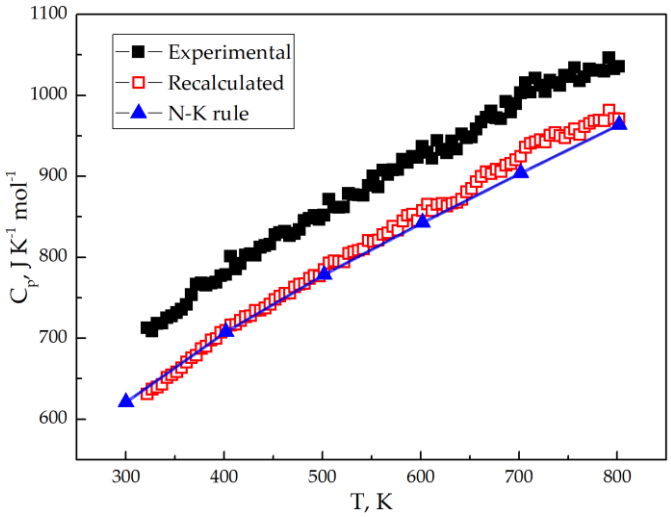

Figure 5. Temperature dependences of the experimental, recalculated and Neumann-Kopp rule heat capacities of $Li_7La_3Zr_2O_{12}$. The line for Neuman-Kopp rule is given as an approximating allometric line.

The Neumann-Kopp rule and recalculated are in good correlation. Experimental data is for LLZO compound with La_2O_3 impurity. The heat capacity temperature dependence (Equation 16) was calculated using tabular data [53], [54]. XRD and EDS quantitative analysis gives accurate enough results for small presence of impurity compounds in material to define it.

4.3. Entropy

Entropy is another thermodynamic function that should be calculated. The Third Law of thermodynamics states, "The entropy of a perfect crystal is zero when the temperature of the crystal is equal to absolute zero (0 K).". Thus, the entropy absolute value can be valued by the equation:

$$S(T) = \int_0^{T_1} \frac{C_p(T)}{T} dT + \frac{\Delta H_1}{T_1} + \int_{T_1}^{T_2} \frac{C_p(T)}{T} dT + \frac{\Delta H_2}{T_2} + \cdots + \int_{T_k}^{T} \frac{C_p(T)}{T} dT, \quad (17)$$

S is entropy, T_k is temperature of the k-th phase transition ($0 < T_k < T$), ΔH_k is enthalpy of the k-th phase transition. Since the entropy can be calculated by Neumann-Kopp rule and if there are no phase transition till calculation temperature, entropy can be also calculated by Neumann-Kopp rule:

$$S(T) = \int_0^{T} \frac{\sum C_p(T, BO)}{T} dT = \sum \int_0^{T} \frac{C_p(T, BO)}{T} dT = \sum S(T, BO), \quad (18)$$

where BO is the binary oxide compound (see eq. (15)). According to eq. (15) and (16), eq. (18) can be written in the following way:

$$S\ (LLZO) = 3{,}5S(Li_2CO_3) + 1.5S(La_2O_3) + 2S(ZrO_2) \quad (19)$$

The entropy of $Li_7La_3Zr_2O_{12}$ at room temperature is 607.18 J mol^{-1} K^{-1} according to eq. (19) and tabular data [53], [54]. Additive rule for entropy calculation is suitable if the sum of the molar volumes of binary compounds differs a bit with the molar volume of the complex compound [54]. Thus, the molar volume for Li_2CO_3 is 35.0 cm^3 mol^{-1} (ϱ=2.11 g cm^{-3} [55]), for La_2O_3 is 50.1 cm^3 mol^{-1} (ϱ=6.51 g cm^{-3} [56]), for ZrO_2 is 21.2 cm^3 mol^{-1} (ϱ=5.56 g cm^{-3} [56]) and for $Li_7La_3Zr_2O_{12}$ is 165.0 cm^3 mol^{-1} (ϱ=5.09 g cm^{-3} [57]). The sum of the molar volumes of Li_2CO_3, La_2O_3 and ZrO_2 with their corresponding stoichiometric coefficients is 240.05 cm^3 mol^{-1} and differs about 45.5% of the LLZO molar volume, which do not allow usage of additive scheme.

Preprints (www.preprints.org) | NOT PEER-REVIEWED | Posted: 10 December 2021 doi:10.20944/preprints202112.0182.v1

Also, the LLZO entropy can be calculated by W.Herz rule [58]:

$$S_{298}^0 = K_H(M/C_{p,298})^{1/3}m, \quad (20)$$

where K_H is Herz constant, M is molar mass, $C_{p,298}$ is isobaric heat capacity, m is atoms per formula.

Herz constant K_H has a good correlation with average values of anion molar mass [58]:

$$K_H = \frac{33.5x^2e^x}{(e^x-1)^2}, \quad (21)$$

where x=42.4/$M_{La_3Zr_2O_{12}}$, M_A is an anion ($La_3Zr_2O_{12}^{7-}$) molar mass. For $Li_7La_3Zr_2O_{12}$, anion molar mass $M_{La_3Zr_2O_{12}}$ is 791.154 g mol^{-1}. Thus, K_H constant is equal to 33.5.

According to eq. (20) and considering $C_{p,298}$ from Table 6 the LLZO entropy is 362.3 J mol^{-1} K^{-1}. Thus, the LLZO entropy calculated by W.Herz rule is not in good correlation with Neumann-Kopp rule result, hence the N-K rule cannot be used for the entropy calculations, as follows from molar masses principle. The calculated value of LLZO entropy by W.Herz rule is in good correlation with Ref. [59].

4.4. The standard Gibbs free energy

The enthalpy of formation and entropy calculated above allows to rate the standard Gibbs energy of LLZO formation (T=298 K):

$$\Delta_f G_{298}^0 = \Delta_f H_{298}^0 - 298\Delta_f S_{298}^0, \quad (22)$$

The resulting value of the Gibbs free energy for $Li_7La_3Zr_2O_{12}$ at room temperature is -9435.6 kJ mol^{-1}.

The next reaction is suggested for determination of stability against metallic lithium with subsequent calculation of the Gibbs free energy at room temperature:

$$3Li + Li_7La_3Zr_2O_{12} = 7.5Li_2O + 1.5La_2O_3 + 2Zr \quad (23)$$

To determine the Gibbs free energy of reaction it is required to subtract from $\Delta_f G_{298}^0$ values of the Gibbs energy for initial reagents of the reaction. The $\Delta_f G_{298}^0$ for single elements is equal to zero, for Li_2O is -561.2 kJ mol^{-1} and for La_2O_3 is -1706.7 kJ mol^{-1} [53]. The $Li_7La_3Zr_2O_{12}$ Gibbs free energy has been calculated above. Thus, the Gibbs free energy for reaction (23) is 8.2 kJ mol^{-1} and this reaction is thermodynamically impossible. Finally, $Li_7La_3Zr_2O_{12}$ is stable against metallic lithium at room temperature.

5. Conclusions

The thermodynamic characteristics were determined for $Li_7La_3Zr_2O_{12}$ solid-state electrolyte material for lithium-ion battery. Solid-state reaction was used as synthesis method of $Li_7La_3Zr_2O_{12}$ from Li_2CO_3, La_2O_3 and ZrO_2. The synthesized material had 3.1 wt. % of the lanthanum oxide (La_2O_3) impurity according to XRD and EDS data. Probably, this amount of La_2O_3 is unreacted oxide during synthesis process. The enthalpy of $Li_7La_3Zr_2O_{12}$ formation from binary oxides (and from Li_2CO_3) $\Delta_{ox}H_{LLZO}$ and from elements Δ_fH_{LLZO} were calculated according to the measured enthalpy of dissolution of reagents and product of $Li_7La_3Zr_2O_{12}$ formation reaction. The obtained values are equal to −186.4 ± 7.3 kJ mol^{-1} and −9327.65 ± 7.9, respectively. The formation enthalpy from binary oxides $\Delta_{ox}H_{LLZO}$ is in good correlation with similar zirconate compounds, which confirms the correctness of the measurements. The $Li_7La_3Zr_2O_{12}$ standard enthalpy of formation from elements is equal - can be used in further thermodynamic modeling and determinations.

The heat capacity value was recalculated considering presence of La_2O_3 impurity. The temperature dependence of the heat capacity is in good correlation with calculated by Neumann-Kopp rule. Finally, the heat capacity can be described by formula $C_p(T)$ = 518.135+0.599 × T - 8.339 × T^{-2}, where T is absolute temperature. The LLZO entropy is equal to 362.3 J mol^{-1} K^{-1}, the Gibbs free energy of $Li_7La_3Zr_2O_{12}$ formation is -9435.6 kJ mol^{-1}. The Gibbs free energy of LLZO reaction with metallic Li is equal to 8.2 kJ mol^{-1}, consequently

$Li_7La_3Zr_2O_{12}$ material is stable against metallic lithium. All thermodynamic values and functions can be used for modelling and further calculations.

Author Contributions: Conceptualization, A.P. and P.N.; methodology, D.A.; software, D.A.; validation, D.A. and Q.W.; formal analysis, A.P.; investigation, D.A.; resources, Q.W.; data curation, P.N.; writing—original draft preparation, D.A.; writing—review and editing, P.N.; visualization, D.A.; supervision, A.P.; project administration, Q.W.; funding acquisition, Q.W. All authors have read and agreed to the published version of the manuscript.

Funding: The research is partially funded by the Ministry of Science and Higher Education of the Russian Federation: Advanced Digital Technologies (contract No. 075-15-2020-934 dated from 17.11.2020)

Institutional Review Board Statement: Not applicable.

Informed Consent Statement: Not applicable.

Data Availability Statement: The data presented in this study are available on request from the corresponding author.

Conflicts of Interest: The authors declare no conflict of interest.

References

1. Nishi, Y. Lithium-ion secondary batteries; past 10 years and the future. *Journal of Power Sources*, **2001**, 100(1-2), 101-106.
2. Ma, J., Li, Y., Grundish, N. S., Goodenough, J. B., Chen, Y., Guo, L., ... & Wan, L. J. The 2021 battery technology roadmap. *Journal of Physics D: Applied Physics*, **2021**, *54*(18), 183001.
3. Horowitz, Y., Schmidt, C., Yoon, D. H., Riegger, L. M., Katzenmeier, L., Bosch, G. M., ... & Golodnitsky, D. Between Liquid and All Solid: A Prospect on Electrolyte Future in Lithium-Ion Batteries for Electric Vehicles. *Energy Technology*, **2020**, 8(11), 2000580.
4. Han, L., Lehmann, M. L., Zhu, J., Liu, T., Zhou, Z., Tang, X., ... & Saito, T. Recent Developments and Challenges in Hybrid Solid Electrolytes for Lithium-Ion Batteries. *Frontiers in Energy Research*, **2020**, *8*, 202.
5. Tan, D. H., Chen, Y. T., Yang, H., Bao, W., Sreenarayanan, B., Doux, J. M., ... & Meng, Y. S. Carbon-free high-loading silicon anodes enabled by sulfide solid electrolytes. *Science*, **2021**, *373*(6562), 1494-1499.
6. Byeon, Y. W., & Kim, H. Review on Interface and Interphase Issues in Sulfide Solid-State Electrolytes for All-Solid-State Li-Metal Batteries. *Electrochem*, **2021**, *2*(3), 452-471.
7. Tripathi, A. K. Ionic liquid based solid electrolytes (ionogels) for application in rechargeable lithium battery. *Materials Today Energy*, **2021**, 100643.
8. Yu, T., Yang, X., Yang, R., Bai, X., Xu, G., Zhao, S., ... & Wang, J. Progress and perspectives on typical inorganic solid-state electrolytes. *Journal of Alloys and Compounds*, **2021**, 161013.
9. Shen, Z., Zhang, W., Zhu, G., Huang, Y., Feng, Q., & Lu, Y. Design Principles of the Anode–Electrolyte Interface for All Solid-State Lithium Metal Batteries. *Small Methods*, **2020**, *4*(1), 1900592.
10. Chan, C. K., Yang, T., & Weller, J. M. Nanostructured garnet-type Li7La3Zr2O12: synthesis, properties, and opportunities as electrolytes for Li-ion batteries. *Electrochimica Acta*, **2017**, *253*, 268-280.
11. Tikekar, M. D., Choudhury, S., Tu, Z., & Archer, L. A. Design principles for electrolytes and interfaces for stable lithium-metal batteries. *Nature Energy*, **2016**, *1*(9), 1-7.
12. Wang, H., Yu, D., Kuang, C., Cheng, L., Li, W., Feng, X., ... & Zhang, Y. Alkali metal anodes for rechargeable batteries. *Chem*, **2019**, *5*(2), 313-338.
13. Famprikis, T., Canepa, P., Dawson, J. A., Islam, M. S., & Masquelier, C. Fundamentals of inorganic solid-state electrolytes for batteries. *Nature materials*, **2019**, *18*(12), 1278-1291.
14. Zhang, Z., Shao, Y., Lotsch, B., Hu, Y. S., Li, H., Janek, J., ... & Chen, L. New horizons for inorganic solid state ion conductors. *Energy & Environmental Science*, **2018**, *11*(8), 1945-1976.
15. Park, K., Yu, B. C., Jung, J. W., Li, Y., Zhou, W., Gao, H., ... & Goodenough, J. B. Electrochemical nature of the cathode interface for a solid-state lithium-ion battery: interface between LiCoO2 and garnet-Li7La3Zr2O12. *Chemistry of Materials*, **2016**, *28*(21), 8051-8059.
16. Murugan, R., Thangadurai, V., & Weppner, W. Fast lithium ion conduction in garnet-type Li7La3Zr2O12. *Angewandte Chemie International Edition*, **2007**, *46*(41), 7778-7781.
17. Bai, Y. X., Zhang, J., Yang, Y. B., Yang, R., Yan, Y. L., & Wang, J. Enhance electrochemical performance of LiFePO4 cathode material by Al-doped Li7La3Zr2O12 and carbon co-coating surface modification. *Journal of Alloys and Compounds*, **2020**, *843*, 154915.
18. Matsui, M., Takahashi, K., Sakamoto, K., Hirano, A., Takeda, Y., Yamamoto, O., & Imanishi, N. Phase stability of a garnet-type lithium ion conductor Li 7 La 3 Zr 2 O 12. *Dalton Transactions*, **2014**, *43*(3), 1019-1024.
19. Dermenci, K. B., Çekiç, E., & Turan, S. Al stabilized Li7La3Zr2O12 solid electrolytes for all-solid state Li-ion batteries. *international journal of hydrogen energy*, **2016**, *41*(23), 9860-9867.

Preprints (www.preprints.org) | NOT PEER-REVIEWED | Posted: 10 December 2021 doi:10.20944/preprints202112.0182.v1

20. Kotobuki, M., Hanc, E., Yan, B., Molenda, J., & Lu, L. Stabilization of cubic Li7La3Zr2O12 by Al substitution in various atmospheres. *Solid State Ionics*, **2020**, *350*, 115323.
21. Polizos, G., Sharma, J., Jafta, C. J., Muralidharan, N., Veith, G. M., Keum, J. K., ... & Wood III, D. L. Nanostructured ligament and fiber Al–doped Li7La3Zr2O12 scaffolds to mediate cathode-electrolyte interface chemistry. *Journal of Power Sources*, **2021**, *513*, 230551.
22. Liu, X., Gao, M., Liu, Y., Xiong, L., & Chen, J. Improving the room temperature ionic conductivity of Al-Li7La3Zr2O12 ceramics by Ba and Y or Ba and W co-doping. *Ceramics International*, **2019**, *45*(10), 13488-13495.
23. Posch, P., Lunghammer, S., Berendts, S., Ganschow, S., Redhammer, G. J., Wilkening, A., ... & Wilkening, H. M. R. Ion dynamics in Al-stabilized Li7La3Zr2O12 single crystals–Macroscopic transport and the elementary steps of ion hopping. *Energy Storage Materials*, **2020**, *24*, 220-228.
24. Matsuki, Y., Noi, K., Suzuki, K., Sakuda, A., Hayashi, A., & Tatsumisago, M. Microstructure and conductivity of Al-substituted Li7La3Zr2O12 ceramics with different grain sizes. *Solid State Ionics*, **2019**, *342*, 115047.
25. Wolfenstine, J., Ratchford, J., Rangasamy, E., Sakamoto, J., & Allen, J. L. Synthesis and high Li-ion conductivity of Ga-stabilized cubic Li7La3Zr2O12. *Materials Chemistry and Physics*, **2012**, *134*(2-3), 571-575.
26. Jalem, R., Rushton, M. J. D., Manalastas Jr, W., Nakayama, M., Kasuga, T., Kilner, J. A., & Grimes, R. W. Effects of gallium doping in garnet-type Li7La3Zr2O12 solid electrolytes. *Chemistry of Materials*, **2015**, *27*(8), 2821-2831.
27. Bernuy-Lopez, C., Manalastas Jr, W., Lopez del Amo, J. M., Aguadero, A., Aguesse, F., & Kilner, J. A. Atmosphere controlled processing of Ga-substituted garnets for high Li-ion conductivity ceramics. *Chemistry of materials*, **2014**, *26*(12), 3610-3617.
28. El Shinawi, H., & Janek, J. Stabilization of cubic lithium-stuffed garnets of the type "Li7La3Zr2O12" by addition of gallium. *Journal of Power Sources*, **2013**, *225*, 13-19.
29. Huang, X., Su, J., Song, Z., Xiu, T., Jin, J., Badding, M. E., & Wen, Z. Synthesis of Ga-doped Li7La3Zr2O12 solid electrolyte with high Li+ ion conductivity. *Ceramics International*, **2021**, *47*(2), 2123-2130.
30. Su, J., Huang, X., Song, Z., Xiu, T., Badding, M. E., Jin, J., & Wen, Z. Overcoming the abnormal grain growth in Ga-doped Li7La3Zr2O12 to enhance the electrochemical stability against Li metal. *Ceramics International*, **2019**, *45*(12), 14991-14996.
31. Shen, L., Wang, L., Wang, Z., Jin, C., Peng, L., Pan, X., ... & Yang, R. Preparation and characterization of Ga and Sr co-doped Li7La3Zr2O12 garnet-type solid electrolyte. *Solid State Ionics*, **2019**, *339*, 114992.
32. Tian, Y., Zhou, Y., Wang, W., & Zhou, Y. Effects of Ga–Ba Co-doping on the morphology and conductivity of Li7La3Zr2O12 electrolyte synthesized by sol-gel method. *Ceramics International*, **2021**.
33. Zhang, Y., Deng, J., Hu, D., Chen, F., Shen, Q., Zhang, L., & Dong, S. Synergistic regulation of garnet-type Ta-doped Li7La3Zr2O12 solid electrolyte by Li+ concentration and Li+ transport channel size. *Electrochimica Acta*, **2019**, *296*, 823-829.
34. Wang, Y., & Lai, W. Phase transition in lithium garnet oxide ionic conductors Li7La3Zr2O12: The role of Ta substitution and H2O/CO2 exposure. *Journal of Power Sources*, **2015**, *275*, 612-620.
35. Chen, X., Wang, T., Lu, W., Cao, T., Xue, M., Li, B., & Zhang, C. Synthesis of Ta and Ca doped Li7La3Zr2O12 solid-state electrolyte via simple solution method and its application in suppressing shuttle effect of Li-S battery. *Journal of Alloys and Compounds*, **2018**, *744*, 386-394.
36. Chen, X., Cao, T., Xue, M., Lv, H., Li, B., & Zhang, C. Improved room temperature ionic conductivity of Ta and Ca doped Li7La3Zr2O12 via a modified solution method. *Solid State Ionics*, **2018**, *314*, 92-97.
37. Guo, H., Su, J., Zha, W., Xiu, T., Song, Z., Badding, M. E., ... & Wen, Z. Achieving high critical current density in Ta-doped Li7La3Zr2O12/MgO composite electrolytes. *Journal of Alloys and Compounds*, **2021**, *856*, 157222.
38. Hosokawa, H., Takeda, A., Inada, R., & Sakurai, Y. Tolerance for Li dendrite penetration in Ta-doped Li7La3Zr2O12 solid electrolytes sintered with Li2. 3C0. 7B0. 3O3 additive. *Materials Letters*, **2020**, *279*, 128481.
39. Huang, X., Xiu, T., Badding, M. E., & Wen, Z. Two-step sintering strategy to prepare dense Li-Garnet electrolyte ceramics with high Li+ conductivity. *Ceramics International*, **2018**, *44*(5), 5660-5667.
40. He, M., Cui, Z., Chen, C., Li, Y., & Guo, X. Formation of self-limited, stable and conductive interfaces between garnet electrolytes and lithium anodes for reversible lithium cycling in solid-state batteries. *Journal of Materials Chemistry A*, **2018**, *6*(24), 11463-11470.
41. Xue, W., Yang, Y., Yang, Q., Liu, Y., Wang, L., Chen, C., & Cheng, R. The effect of sintering process on lithium ionic conductivity of Li 6.4 Al 0.2 La 3 Zr 2 O 12 garnet produced by solid-state synthesis. *RSC Advances*, **2018**, *8*(24), 13083-13088.
42. Huang, X., Song, Z., Xiu, T., Badding, M. E., & Wen, Z. Sintering, micro-structure and Li+ conductivity of Li7− xLa3Zr2− xNbxO12/MgO (x= 0.2–0.7) Li-Garnet composite ceramics. *Ceramics International*, **2019**, *45*(1), 56-63.
43. Yang, T., Li, Y., Wu, W., Cao, Z., He, W., Gao, Y., ... & Li, G. The synergistic effect of dual substitution of Al and Sb on structure and ionic conductivity of Li7La3Zr2O12 ceramic. *Ceramics International*, **2018**, *44*(2), 1538-1544.
44. Xiang, X., Chen, F., Shen, Q., Zhang, L., & Chen, C. Effect of the lithium ion concentration on the lithium ion conductivity of Ga-doped LLZO. *Materials Research Express*, **2019**, *6*(8), 085546.
45. Chen, F., Zhang, Y., Hu, Q., Cao, S., Song, S., Lu, X., & Shen, Q. S/MWCNt/LLZO Composite Electrode with e-/S/Li+ Conductive Network for All-Solid-State Lithium–Sulfur Batteries. *Journal of Solid State Chemistry*, **2021**, 122341.
46. Goswami, N., Indu, M. S., Murugan, R., & Kant, R. Experimental corroboration of theory for impedance response of solid electrolytes: Doped cubic garnet LLZO. *Journal of Electroanalytical Chemistry*, **2021**, *897*, 115611.
47. Aravinth, K., Ramasamy, P., Sen, S., & Arumugam, R. Tunable photoluminescence properties of Dy3+ doped LLZO phosphors for WLED and dosimetry applications. *Ceramics International*, **2021**.
48. Samui, P., Modi, K. B., Phapale, S., Parida, S. C., & Mishra, R. Calorimetric investigations on lithium based ceramics. *The Journal of Chemical Thermodynamics*, **2021**, *163*, 106590.

Preprints (www.preprints.org) | NOT PEER-REVIEWED | Posted: 10 December 2021 doi:10.20944/preprints202112.0182.v1

49. Wyers, G. P., Cordfunke, E. H. P., & Ouweltjes, W. The standard molar enthalpies of formation of the lithium zirconates. *The Journal of Chemical Thermodynamics*, **1989**, *21*(10), 1095-1100.
50. Bolech, M., Cordfunke, E. H. P., Van Genderen, A. C. G., Van Der Laan, R. R., Janssen, F. J. J. G., & Van Miltenburg, J. C. The heat capacity and derived thermodynamic functions of La2Zr2O7 and Ce2Zr2O7 from 4 to 1000 K. *Journal of Physics and Chemistry of Solids*, **1997**, *58*(3), 433-439.
51. Wang, M., Navrotsky, A., Venkatraman, S., & Manthiram, A. Enthalpy of Formation of Li x CoO2 (0.5⩽ x⩽ 1.0). *Journal of the Electrochemical Society*, **2005**, *152*(7), J82.
52. Huntelaar, M. E., Booij, A. S., & Cordfunke, E. H. P. The standard molar enthalpies of formation of BaZrO3 (s) and SrZrO3 (s). *The Journal of Chemical Thermodynamics*, **1994**, *26*(10), 1095-1101.
53. Glushko V.P., Gurvich L.V., Bergman G.A., Veits I.V., Medvedev V.A., Khachkuruzov G.A., Yungman V.S. Thermodinamicheskie Svoitsva Individual'nykh Veshchestv; Nauka: Moscow, Russia, **1978**, URL: "http://twt.mpei.ac.ru/TTHB/2/OIVT/IVTAN-Thermo/Eng/index.htm".
54. Pankratz, L. B. Thermodynamic properties of carbides, nitrides, and other selected substances, **1995**, ISBN-10: 9995679329, URL: "ark:/67531/metadc12836".
55. Lide, D.R. CRC Handbook of Chemistry and Physics 86TH Edition 2005-2006. CRC Press, Taylor & Francis, Boca Raton, FL **2005**, p. 4-70, ISBN: 0849304865 9780849304866.
56. G.V. Samsonov, The oxide handbook, Springer, US (**1973**), ISBN: 978-1-4615-9597-7, URL: "https://doi.org/10.1007/978-1-4615-9597-7".
57. Awaka, J., Kijima, N., Hayakawa, H., & Akimoto, J. Synthesis and structure analysis of tetragonal Li7La3Zr2O12 with the garnet-related type structure. *Journal of solid state chemistry*, **2009**, *182*(8), 2046-2052.
58. Morachevskiy A. G., Sladkov I. B., Firsova Ye. G. Termodinamicheskiye raschety v khimii i metallurgii; Lan': St.Petersburg, Russia, **2018**, ISBN: 978-5-8114-3023-9.
59. Il'ina, E. A., Raskovalov, A. A., & Reznitskikh, O. G. Thermodynamic properties of solid electrolyte Li7La3Zr2O12. *The Journal of Chemical Thermodynamics*, **2019**, *128*, 68-73.